Applied Surface Science 389 (2016) 1182–1191

Contents lists available at ScienceDirect

Applied Surface Science

journal homepage: www.elsevier.com/locate/apsusc

Effect of Cr on the passive film formation mechanism of steel rebar in saturated calcium hydroxide solution

Ming Liu [a], Xuequn Cheng [a], Xiaogang Li [a,b,*], Yue Pan [a], Jun Li [a]

[a] Corrosion and Protection Center, University of Science and Technology Beijing, Beijing, 100083, China
[b] Ningbo Institute of Material Technology & Engineering, Chinese Academy of Sciences, Ningbo, 315201, Zhejiang, China

ARTICLE INFO

Article history:
Received 9 June 2016
Received in revised form 13 August 2016
Accepted 18 August 2016
Available online 21 August 2016

Keywords:
Chromium
Rebar
Passive film
XPS
AES

ABSTRACT

Passive films grow on the surface of Cr-modified steels subjected to saturated $Ca(OH)_2$ solution. Electrochemical techniques, such as measurement of open circuit potentials, polarization curves, and electrochemical impedance spectroscopy combined with X-ray photoelectron spectrometer and auger electron spectroscopy, were applied to study the influence of low Cr content on the passive film formation mechanism of steel rebar in saturated $Ca(OH)_2$ solution. Results show that Cr inhibits the formation of passive film at the beginning of its formation. Corrosion current density decreases and polarization resistance increases with the extension of the immersion time. A stable passive film takes at least three days to form. The passive film resistance of HRB400 carbon steel is higher than that of Cr-modified steels in the early stage of immersion (<72 h). The polarization resistance of Cr-modified steel is larger after a stable passive film is formed (>72 h), and Cr promotes the formation of a denser and more compact passive film. The stable passive film is primarily made up of iron oxides with a thickness of 5–6 nm. Cr are involved in the formation of passive films, thereby resulting in a film that consists of an inner layer that contains Cr–Fe oxides and an outer layer that contains Fe oxides, whose thickness presents a slight increase as the content of Cr increases.

1. Introduction

Carbon steel rebars have excellent corrosion resistance in concrete because of passive film formation in a high alkaline environment (pH = 12–13), thereby protecting the rebar from corrosion [1–3]. The passive film of carbon steel rebar in concrete has a bilayer structure; the inner is primarily made up of inadequately oxidized Fe_3O_4, while the outer layer is made up of γ-Fe_2O_3. The passive film of stainless steel rebar is a bilayer rich in Cr, with the intimal layer containing Cr oxides and the outer layer containing Fe oxides [4–6]. Mancio et al. [7] reported that a bilayer film that contains Cr is also likely to form on the surface of a MMFX steel rebar with 9% Cr. Results of surface enhanced laser Raman spectroscopy indicate that the inside layer contains $Cr(OH)_3$, while the outside is composed of Fe_3O_4, γ-Fe_2O_3, and α-FeOOH. The existence of $Cr(OH)_3$ is crucial to the significant enhancement of the corrosion resistance, which is distinguished from the passive film of the carbon steel.

To date, little attention has been paid to the passivation behavior and effect of corrosion-resistant steel rebar, and the conclusions are not unified. The carbonation and erosion of Cl^- have an important influence on the destruction of the passive film of steel bars [2,6,8–11]. In fact, apart from pH and Cl^-, passivation time is also important to the formation of a passive film. OH^- plays a role in advancing and maintaining passivation, while Cl^- has inhibition and destruction effects, leading to a competition between passivation and transpassivation [8–11]. As a result, the degrees of passivation and transpassivation are time varying. Furthermore, the formation and dissolution of the passive film in an alkaline environment are mutually reversible and simultaneous. On the one hand, the passive film grows toward the matrix. On the other hand, the passive film dissolves on the film/solution interface. The passive film achieves a stable state and the thickness remains almost invariable when the dissolution and formation reach dynamic equilibrium [12–14]. A completely stable passive film for carbon steel in room temperature, which may be distinct from that of low-alloy corrosion resistant steel rebar on account of the specific characteristics of its passivation behavior accompanied with the dissolution of Fe and Cr takes 3 and 7 days to form [15,16], respectively, in a non-carbonated and non-chloride polluted simulated concrete pore solution and mortar. Nevertheless, the assessment and characterization of the passivation of corrosion resistant rebar with various passivation times have not been reported yet, and the variation of composition, structure, and electrochemical properties remain to be explored.

* Corresponding author at: Corrosion and Protection Center, University of Science and Technology Beijing, Beijing, 100083, China.
E-mail address: lixiaogang@ustb.edu.cn (X. Li).

http://dx.doi.org/10.1016/j.apsusc.2016.08.074
0169-4332/

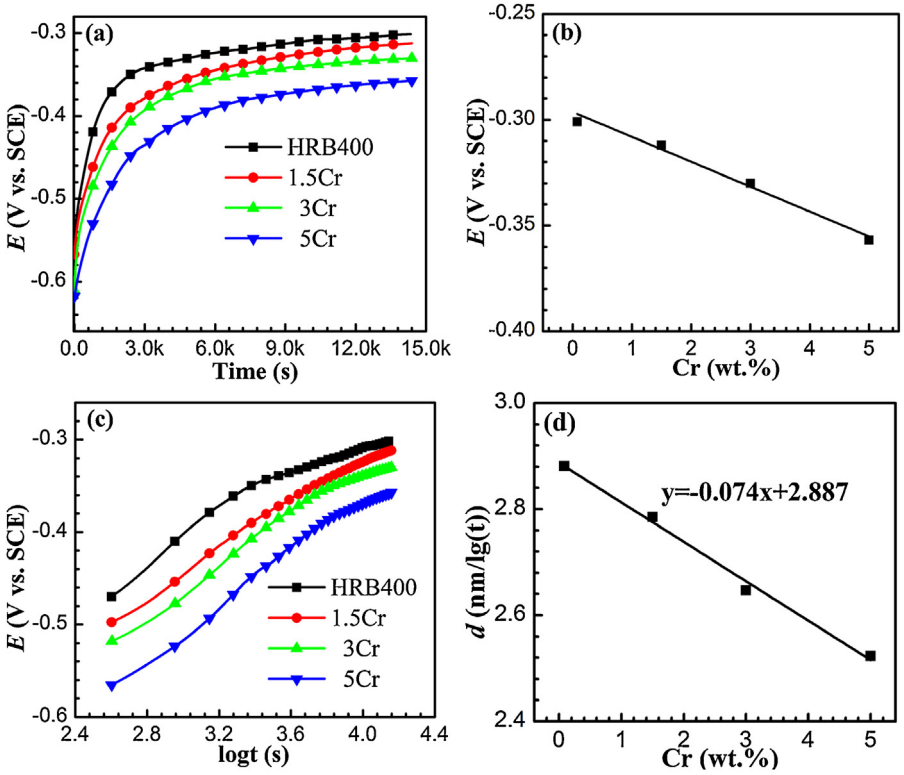

Fig. 1. (a) OCP, *E*, of the steels electrode with 4 h in CH solutions; (b) OCP at 4 h, (c) OCP vs. logt, (d) the initial formation rate of passive film of rebar after 4 h of immersion in CH solution.

Table 1
Chemical composition (wt.%) of the tested HRB400 carbon steel and Cr-modified steels.

Steel	C	Si	Mn	P	S	Cr	Fe
HRB400	0.196	0.57	1.57	0.024	0.017	0.08	residual
1.5Cr	0.171	0.66	1.30	0.014	0.008	1.50	residual
3Cr	0.184	0.65	1.23	0.007	0.012	3.02	residual
5Cr	0.157	0.45	1.57	0.010	0.004	5.06	residual

Our previous work studied the corrosion behavior of Cr-modified low alloy steel rebar in saturated $Ca(OH)_2$ solution [17]. Cr-modified low alloy steels show excellent corrosion resistance with higher critical chloride concentrations and lower average corrosion rates. However, the effect of Cr on the passive film formation process is unclear. This paper is anticipated to validate the effect of Cr on the composition and mechanism of corrosion resistance to compensate for the deficiency of our previous work. The passive behavior in saturated $Ca(OH)_2$ solution with various passive time was investigated through electrochemical techniques. Passive film composition was investigated with X-ray photoelectron spectrometer (XPS) and auger electron spectroscopy (AES).

2. Experimental

2.1. Materials and solution

In this work, HRB400 carbon steel rebar and three Cr-modified low alloy steel rebars were used for experiments [17]. Table 1 shows the chemical composition (in% by mass) of the four kinds of steel rebars determined by analytical analysis. The specimens for electrochemical tests with dimensions of $10 \times 10 \times 5$ mm, and the exposed measurement area was 10×10 mm retained by the epoxy resin. Prior to the experiment, the samples were polished with silicon carbide (SiC) water polishing papers down to 2000#, then ultrasonically cleaned in acetone and rinsed in distilled water.

The saturated $Ca(OH)_2$ (CH) solution [1,2,8,17–19] was chosen to simulate the concrete pore solution in present work. The excess CH was dissolved in deionized water, and the supernatant was taken as the experimental solution.

2.2. Electrochemical measurements

The electrochemical measurements were carried out with the Partstat 2273 Advanced Potentiostat/Galvanostat/FRA system with a three-electrode cell system, while the steel rebars acted as a working electrode, a saturated calomel electrode (SCE) as a reference electrode and a platinum plate as a counter electrode.

The polarization curves were recorded potentiodynamically with a scanning rate of 1 mV/s, starting from −0.25 V vs. OCP to transpassive potential. The electrochemical impedance spectroscopy (EIS) data were obtained with the frequency range from 100 kHz to 10 mHz and a sinusoidal potential perturbation of 10 mV at the open circuit potentials. The experimental results were interpreted based on an equivalent electrical circuit by using a suitable fitting procedure of ZsimpWin. The capacitance measurements were performed on the films at a fixed frequency of 1 kHz during a 40 mV/Step in the potential range from −1.0 V to 1.0 V (vs. SCE). All measurements were carried out at ambient temperature approximately 25 °C.

2.3. XPS analysis

The chemical composition of the steel rebars passive films were investigated by X-ray photoelectron spectrometer (XPS) with a monochromatic Al K_a radiation source and a hemispherical electron analyzer operated at a pass energy of 25 eV. The element compo-

sition and content were analyzed by comparing with the standard spectra of elements which are from XPS company's Perkin-Elmer data handbook and International Inc. XPS website. The curve fitting was performed with the commercial software Xpspeak version 4.1 and Gaussian-Lorentzian tail function for better spectra fitting.

2.4. AES measurements

AES tests were performed on a PHI-700 (ULVAC-PHI) equipped with a coaxial electron gun and a cylindrical mirror analyzer (CMA). Auger spectra were taken at 5 keV with an energy resolution of 0.1%. AES analysis was performed in a surface analysis chamber with a base vacuum of 3.9×10^{-9} Torr. The electron incidence angle with respect to the normal average surface plain was 30°. All samples were sputtered with Ar^+ ions for 0.5 min to remove surface contamination from air handling. The sputtering rate, as determined on a thermal oxidation SiO_2/Si standard, was approximately 1 nm/min. The major peaks selected for the AES study were Fe (701 eV), Cr (529 eV), O (503 eV).

3. Results and discussion

3.1. Open circuit potential

Fig. 1(a) shows the open circuit potential (OCP) of the steel rebars in the initial measured 4 h, which shows that the addition of Cr mitigates the formation of the passive film in CH solution. The OCP of steels that contain various Cr contents at 4 h are shown in Fig. 1(b), thereby indicating that the OCP exhibits a linear decline with the increasing Cr content. The initial formation rate of passive film in CH solution can be characterized by the variation of the OCP with time [20]. The following formula was adopted to calculate the initial formation rate of passive film:

$$E = \text{const.} + 2.303\delta^-/A \log t \quad (1)$$

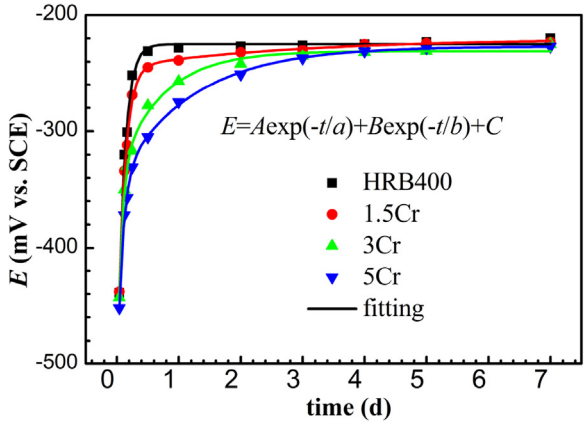

Fig. 2. Variation of OCP with time of steel rebars in CH solution.

Where δ^-delegates the rate of passive film developing per unit decade of time, and A is a constant, which can be expressed as [21]:

$$A = \frac{nF}{RT}\alpha\delta' \quad (2)$$

where α is the transfer coefficient ($0 < \alpha < 1$), δ^- is the width of the ion transfer on the energy barrier, n equals to 2, and the calculated *A* amounts to 39 nm/V. The *E*-log*t* diagram along with 4 h in Fig. 1(c) illustrates that a significant linear relationship exists. The passive film growth rate of the Cr-modified steel could be calculated using formula (1). Fig. 1(d) shows the relationship of oxide film thickening, *d*, and Cr content, which is represented by a straight line with a slope of 0.074 nm/lg*t*. This finding indicates that adding Cr element to steel inhibits the initial passive film formation in CH solution.

Fig. 2 shows the variation curve of OCP with time of steel rebars immersed for 7 d in CH solution. The OCP of the HRB400 and 1.5 Cr steels reach approximately −250 mV (vs. SCE) after immersion for

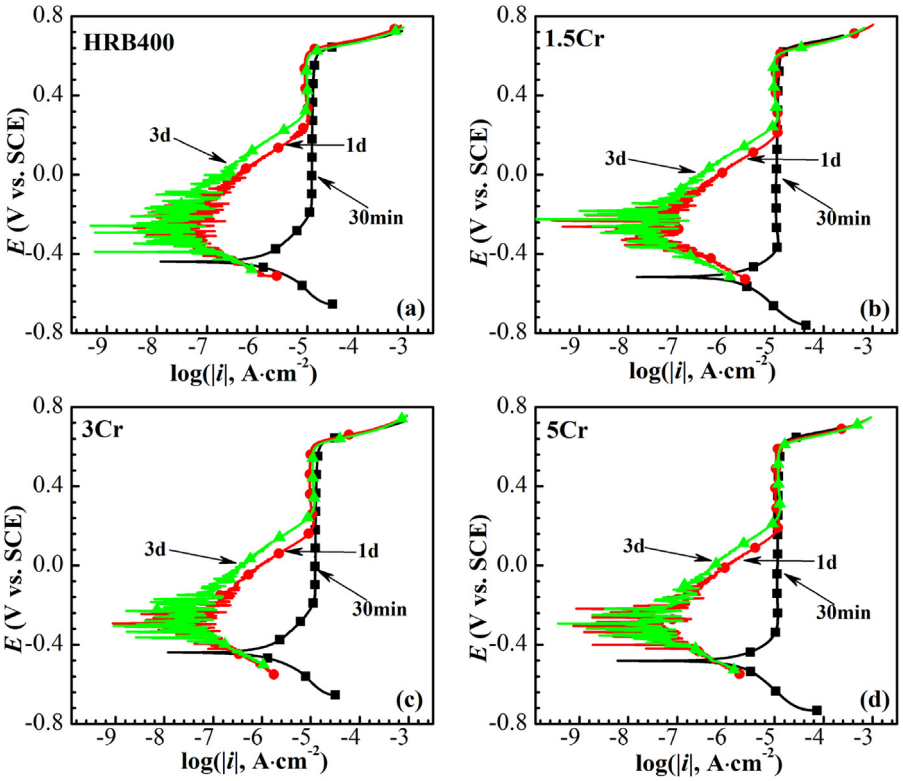

Fig. 3. The polarization curves of steel rebars immersed for different time in CH solution: (a) HRB400, (b) 1.5 Cr, (c) 3 Cr, (d) 5 Cr.

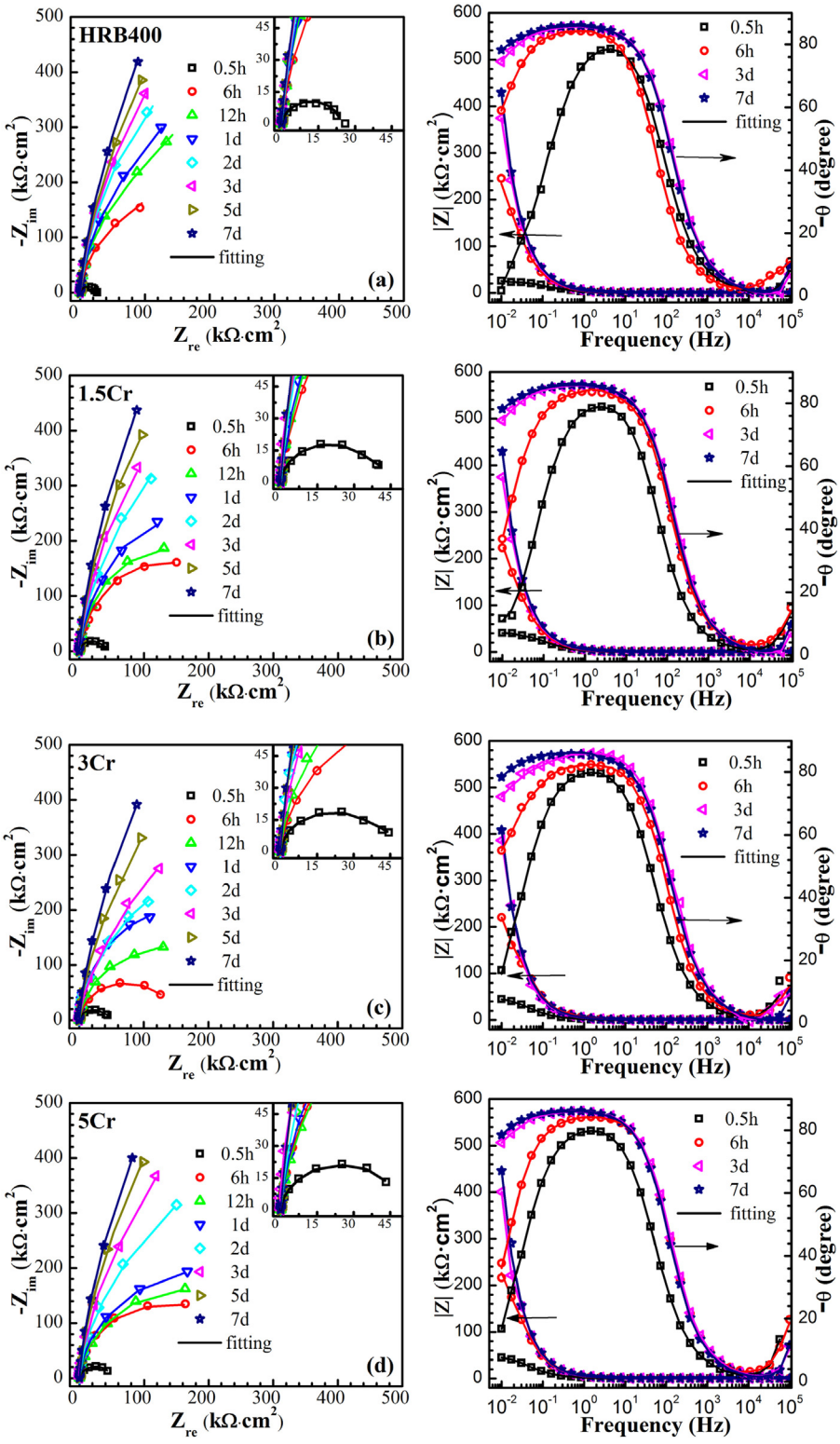

Fig. 4. Nyquist plots and bode plots for the specimens in CH solution immersed for different time: (a) HRB400, (b) 1.5 Cr, (c) 3 Cr, (d) 5 Cr.

1 day and after 3 days for 3 Cr and 5 Cr steels. Subsequently, the OCP remains relatively stable with a slight fluctuation.

According to Sanchez [22], the variation of OCP with time of carbon steel in CH + 0.2 M NaOH solution demonstrates the following functional relationship:

$$E = A\exp(-t/a) + B\exp(-t/b) + C \quad (3)$$

where A, B, C, a, and b are all constants. On the basis of (3), the variation curves were fitted, and the fitting results are shown in Fig. 2 and Table 2, which illustrate that the relationship in formula (3) is credible and the formation of a passive film is in accordance with the exponent function law.

Table 2
Fitting results of OCP versus time in CH solution.

Steel	Fitting results	R^2
HRB400	$E = -153.41 \cdot \exp(-t/0.11) - 153.41 \cdot \exp(-t/0.11) - 225.02$	0.9945
1.5Cr	$E = -275.36 \cdot \exp(-t/0.11) - 24.99 \cdot \exp(-t/2.86) - 220.12$	0.9982
3Cr	$E = -203.97 \cdot \exp(-t/0.07) - 106.29 \cdot \exp(-t/0.72) - 230.86$	0.9948
5Cr	$E = -178.13 \cdot \exp(-t/0.09) - 115.98 \cdot \exp(-t/1.21) - 226.80$	0.9993

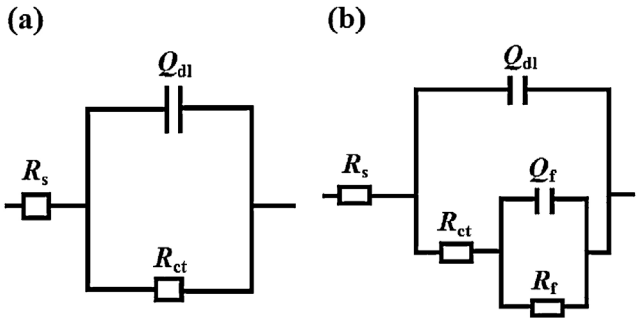

Fig. 5. Equivalent circuits of the EIS used in the experiment.

3.2. Polarization curves

Fig. 3 shows the polarization curve of steels immersed for different time in CH solution. It can be seen that the polarization curves exhibit typical passive characteristics. The curves of the four types of steel after immersion for 30 min are analogous in shape with a wide passive range. The anodic polarization curve directly goes into the passive region without any features of transformation from activation. The shapes of the curves of the steels are also similar after 1 day of immersion. Overall, the curves shift up to the left. The corrosion potential, E_{corr}, moves to the positive direction, and the self-corrosion current density, i_{corr}, decreases with the extension of the immersion time, which means that the corrosion rate is lower. After immersion for 1d, the corrosion current densities of the four kinds of steels are all less than 0.1 $\mu A/cm^2$, which demonstrates that the protective passive film formed on the surface of steel rebars after being immersed in CH solution for 1 day.

3.3. EIS

The EIS diagrams of rebars immersed for different times in CH solution are displayed in Fig. 4; the left side is the Nyquist diagram, while the right is part of the corresponding Bode diagram. The radius of capacitive loop is magnified gradually as the immersion time increases. Therefore, the corrosion resistance of the passive film is enhanced. The Bode diagram of steels immersed for 30 min presents a capacitive loop with one time constant, whereas that immersed for 6 h is broadened and enlarged, thereby indicating the existence of at least two time constants [17,18,23].

The equivalent circuit in Fig. 5 is established to fit the parameters of EIS in Fig. 4 [8,9,18,23], where Fig. 5(a) is for the specimens immersed for 30 min and Fig. 5(b) for the specimens immersed for over 6 h. R_s is the solution resistance from the reference electrode to the working electrode, R_{ct} is the charge transfer resistance, Q_{dl} is the constant phase angle element of the electric double-layer capacitor, R_f stands for the forming resistance of the outside layer of passive film, and Q_f is the constant phase angle element of the outside layer of the passive film. The impedance values of the equivalent circuit in (a) and (b) are expressed in Eqs. (4) and (5), respectively.

$$Z = R_s + \frac{1}{Z_{Q_{dl}} + \frac{1}{R_{ct}}} \tag{4}$$

$$Z = R_s + \frac{1}{Z_{Q_{dl}} + \frac{1}{R_{ct} + \frac{1}{Z_{Q_f} + \frac{1}{R_f}}}} \tag{5}$$

In general, the capacitor of the electric double layer cannot be considered as the ideal capacitive element because of the roughness of the electrode surface, the impedance of which is always concerned with the angular frequency of the pumping signals and conveyed in the following form:

$$Z_{Q_{dl}} = \frac{1}{Y_0(j\omega)^n} \tag{6}$$

where Y_0 is a proportional factor, ω is the angular frequency, j is the symbol for imaginaries, and n represents the index of the constant phase angle element ranging from 0.5 to 1. The element is equivalent to a capacitor when n = 1 [8,9,17,18,23]. Q_f and Q_{dl} have similar meanings.

Tables 3–6 show the fitting value parameters in the EIS diagram of steels through the ZsimpWin software, and Fig. 6 shows the variation of R_{ct} and R_f with time. Cr-modified steels possess relatively larger R_{ct} when immersed for 30 min, and R_{ct} increases slightly with the extension of the immersion time, which proves the reasonability of the equivalent circuit in Fig. 5(b). Fig. 6(b) shows that R_f increases rapidly as immersing time elapses, demonstrating that a protective passive film emerges swiftly. In the first three days, the R_f of the HRB400 steel is higher than that of Cr-modified steels, that is, the formation rate of passive film is higher. After immersion for three days, the formation rate of passive film slows down progressively; R_f of passive film of Cr-modified steels is higher than that of the HRB400, and 5Cr steel possesses the highest R_f. Therefore, Cr helps form a more protective passive film in the later period because the migration rate of Cr in the passive film is relatively slow [12,24,25]. Specifically, Fe oxides occupy the dominant position and Cr inhibits the dissolution of Fe in the initial formation, consequently causing a lower R_f, while R_f increases as a result of the formation of Fe–Cr oxides afterwards [3–5,12].

In electrochemical impedance spectroscopy theory, $R_p = R_{ct}+R_f$ is adopted to calculate the polarization resistance of rebars in simulated concrete pore solution [9,18,26]. R_p increases and reaches the order of magnitude of $10^6\ \Omega\,cm^2$ as immersing time elapses when immersed for seven days. In addition, R_p can be enhanced by adding Cr. Hence, a stable and compact passive film can be fromed on the surface of the Cr-modified low alloy steel in CH solution.

3.4. Capacitance results

The semiconducting properties of the steel rebar passive films were investigated through capacitance measurements, which can be described with the Mott-Schottky equation as follows [26,28–30]:

$$\frac{1}{C^2} = +\frac{2}{\varepsilon\varepsilon_0 eN}(E - E_{fb} - \frac{kT}{e}) \tag{7}$$

where the positive sign is for n-type and the negative sign is for p-type conductivity; C represents for the semiconductor electrode under depletion condition; and e is the electron charge, N charge carrier density, the donor density for n-type or the acceptor density for p-type semiconductors, ε_0 the vacuum permittivity, ε the

Table 3
Fitting parameters of EIS in CH solution (HRB400).

Time, h	R_s, Ω cm^2	R_{ct}, kΩ cm^2	Q_{dl},		R_f, kΩ cm^2	Q_f,	
			Y_0 Ω^{-1} cm^{-2} s^n	n		Y_0 Ω^{-1} cm^{-2} s^n	n
0.5	46.1	24.3	55.7×10^{-6}	0.92	–	–	–
6	47.1	30.4	23.5×10^{-6}	0.93	429.2	12.7×10^{-6}	0.98
12	47.3	37.9	23.1×10^{-6}	0.98	1004.1	12.3×10^{-6}	0.97
24	47.8	43.2	22.1×10^{-6}	0.96	1160.2	11.7×10^{-6}	0.96
48	49.8	47.6	16.2×10^{-6}	0.98	1711.2	10.1×10^{-6}	0.90
72	50.3	52.3	15.9×10^{-6}	0.95	2261.5	9.7×10^{-6}	0.98
120	50.6	53.5	15.1×10^{-6}	0.97	2767.4	9.1×10^{-6}	0.98
168	52.3	55.7	14.0×10^{-6}	0.98	3034.9	8.8×10^{-6}	0.90

Table 4
Fitting parameters of EIS in CH solution (1.5Cr).

Time, h	R_s, Ω cm^2	R_{ct}, kΩ cm^2	Q_{dl},		R_f, kΩ·cm^2	Q_f,	
			Y_0 Ω^{-1} cm^{-2} s^n	n		Y_0 Ω^{-1} cm^{-2} s^n	n
0.5	50.3	33.7	48.0×10^{-6}	0.94	–	–	–
6	51.1	36.7	36.1×10^{-6}	0.94	595.2	9.6×10^{-6}	0.97
12	51.6	39.3	24.2×10^{-6}	0.99	830.0	9.2×10^{-6}	0.98
24	52.3	45.5	23.5×10^{-6}	0.91	929.3	8.9×10^{-6}	0.99
48	54.2	52.0	22.9×10^{-6}	0.96	1531.1	8.6×10^{-6}	0.99
72	56.7	54.6	18.1×10^{-6}	0.96	2049.8	8.3×10^{-6}	0.97
120	56.3	57.6	17.1×10^{-6}	0.95	2902.1	8.1×10^{-6}	0.97
168	57.1	60.4	16.5×10^{-6}	0.97	3190.7	7.5×10^{-6}	0.95

Table 5
Fitting parameters of EIS in CH solution (3Cr).

Time, h	R_s, Ω cm^2	R_{ct}, kΩ cm^2	Q_{dl},		R_f, kΩ cm^2	Q_f,	
			Y_0 Ω^{-1} cm^{-2} s^n	n		Y_0 Ω^{-1} cm^{-2} s^n	n
0.5	45.7	41.6	50.4×10^{-6}	0.92	–	–	–
6	46.3	45.8	36.4×10^{-6}	0.98	586.6	23.9×10^{-6}	0.94
12	46.5	46.2	27.1×10^{-6}	0.97	600.8	21.8×10^{-6}	0.93
24	47.8	49.7	24.8×10^{-6}	0.93	756.7	22.1×10^{-6}	0.96
48	48.3	55.6	16.5×10^{-6}	0.95	1436.9	16.1×10^{-6}	0.96
72	49.7	57.3	15.7×10^{-6}	0.97	2220.8	15.7×10^{-6}	0.99
120	50.4	60.8	13.9×10^{-6}	0.96	3043.3	15.6×10^{-6}	0.92
168	51.8	65.3	12.3×10^{-6}	0.99	3368.7	15.1×10^{-6}	0.94

Table 6
Fitting parameters of EIS in CH solution (5Cr).

Time, h	R_s, Ω cm^2	R_{ct}, kΩ cm^2	Q_{dl},		R_f, kΩ cm^2	Q_f,	
			Y_0 Ω^{-1} cm^{-2} s^n	n		Y_0 Ω^{-1} cm^{-2} s^n	n
0.5	44.8	49.3	54.5×10^{-6}	0.92	–	–	–
6	45.2	50.1	32.9×10^{-6}	0.94	369.7	23.7×10^{-6}	0.82
12	45.4	52.3	31.8×10^{-6}	0.95	432.6	21.0×10^{-6}	0.93
24	45.8	56.2	31.1×10^{-6}	0.93	757.7	19.8×10^{-6}	0.98
48	46.3	57.9	29.2×10^{-6}	0.99	1595.7	12.7×10^{-6}	0.93
72	46.7	60.4	28.3×10^{-6}	0.98	2147.3	12.2×10^{-6}	0.92
120	47.1	64.5	17.9×10^{-6}	0.98	3218.8	11.5×10^{-6}	0.93
168	47.8	68.3	16.2×10^{-6}	0.97	3474.7	9.8×10^{-6}	0.96

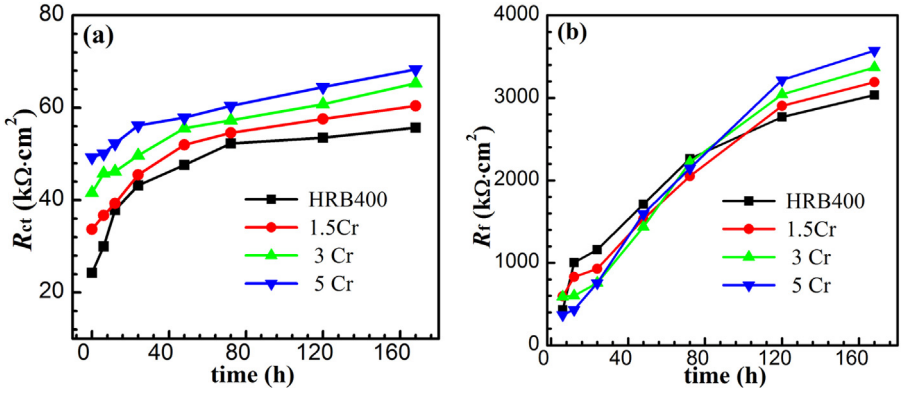

Fig. 6. Variations of the Charge transfer resistance, R_{ct}, (a) and passive film resistance, R_f, (b) for the specimens immersed in CH solution for different time.

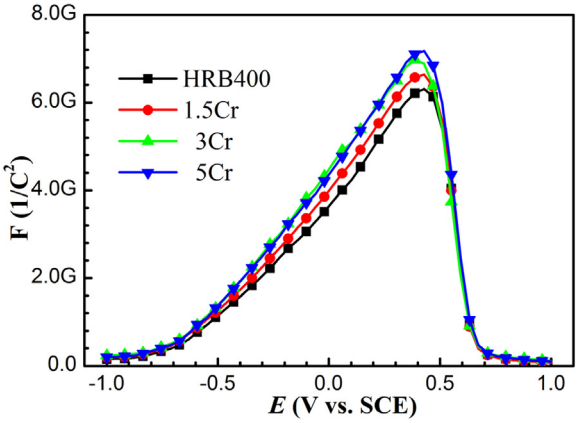

Fig. 7. Mott–Schottky curves of the steel rebars in CH solution.

relative dielectric constant of the semiconductor, k Boltzmann's constant and T absolute temperature; E is the applied electrode potential and E_{fb} is the flat band potential. Fig. 7 displays the Mott-Schottky plots of HRB400 steel and Cr modified steels in CH solution at the OCP. Obviously, the curves are divided into two regions in the light of membrane formation potential. For potential from −600 mV to +500 mV, the plots of the HRB400 steel and Cr-modified steels show linear relationship with a positive slope, which means that the passive films behave as an n-type semiconductor. This is in accordance with the previous study on passive film of carbon steel rebar in alkaline solution [29,30]. In addition, for the potential more postive than 500 mV, the slope of the plots turns to negative. This is due to the enhancement of the conductivity of the oxides, resulting in the conversion of passive film from N type to the P type

Table 7
Donor densities of the passive films on steel rebars in CH solution.

Steel	HRB400	1.5 Cr	3 Cr	5 Cr
$N_D/10^{21}cm^{-3}$	2.01	1.94	1.82	1.81

[26,28–30]. The concentration of the electron donor, N_d, can be calculated from the positive slope of the C^{-2} vs. E curves [28–30].

$$N = \frac{2}{m \cdot e \cdot \varepsilon \cdot \varepsilon_0} \quad (8)$$

where m is the slope of the Mott–Schottky plots in the region of Linear; e is the electron charge, $e = 1.602 \times 10^{-19}$C; ε_0, the vacuum permittivity,$\varepsilon_0 = 8.85 \times 10^{-12}$F/m; ε, the relative dielectric constant of the semiconductor, $\varepsilon = 12$[29,30]. Table 7 shows the values of N_d in the order of magnitude of 10^{21} cm^{-3}, which is consistent with previous work [27–30]. Besides, the value of N_d decreases with the increase in Cr content. Thus, the passive film of Cr-modified steels have better stability, which is consistent with the measurement results of EIS.

3.5. XPS results

The passive film chemical constitution may have significant effects on passivation characteristics. Figs. 8–10 present the XPS spectra HRB400 and Cr modified steels passive films that formed at the OCP immersed in CH solution for 7 days, thereby illustrating that the dominant components of the oxides in CH solutions are iron oxide and chromium oxide species, respectively. According to the method reported in the literature [12,26,27,31], the different state of oxides are fitted.

From Fig. 8, it can be seen that the iron profile performs primary four peaks: Fe^{3+} in hydroxide form (713.47 eV) and in oxide form (711.58 eV), Fe^{2+} oxides (710.18 eV), and Fe^0 (met) (708.04 eV) for the HRB400 steel and Cr-modified steel rebars. Fe^0 (708.04 eV)

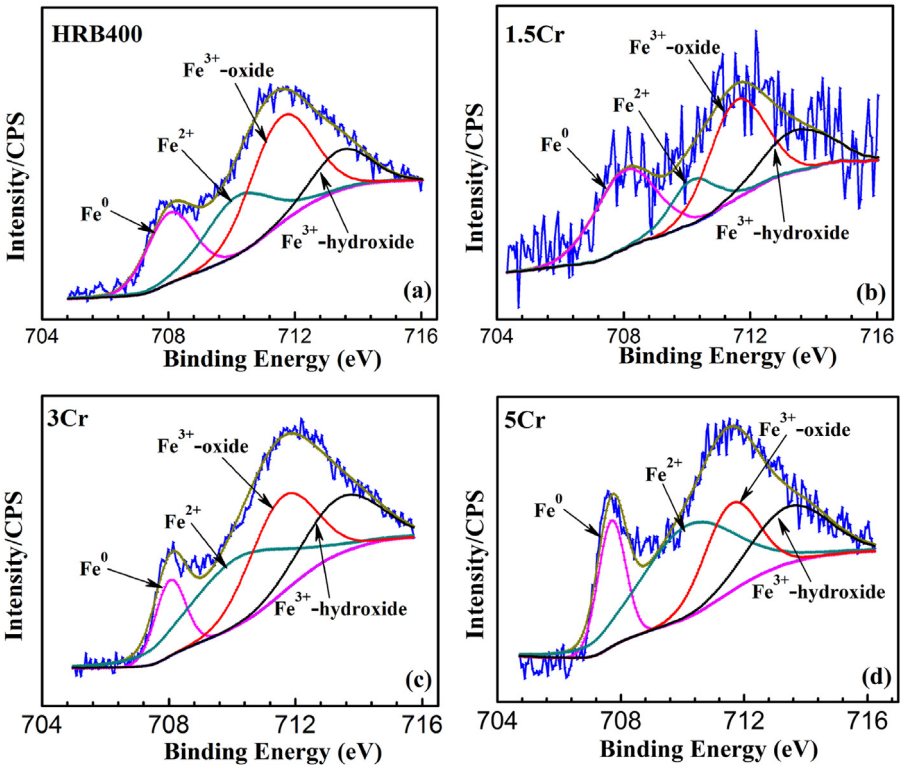

Fig. 8. Fe2p3/2 peak fitting of steel rebars after immersion in CH solution [17]. (a) HRB400, (b) 1.5 Cr, (c) 3 Cr, (d) 5 Cr.

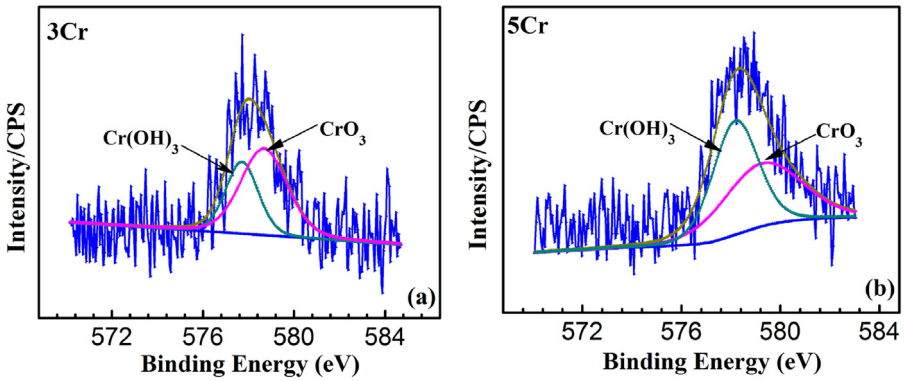

Fig. 9. Cr2p3/2 peak fitting of steel rebars after immersion in CH solution [17]. (a) 3 Cr, (b) 5 Cr.

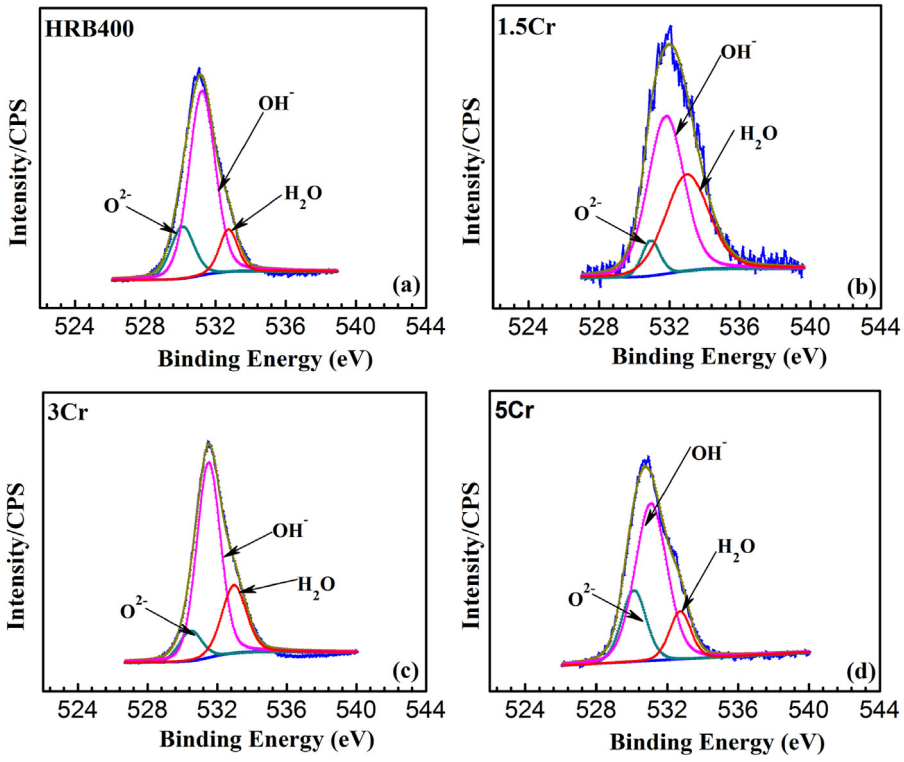

Fig. 10. O1s peak fitting of steel rebars after immersion in CH solution [17]. (a) HRB400, (b) 1.5 Cr, (c) 3 Cr, (d) 5 Cr.

could be detected in the HRB400 steel and Cr-modified steel rebars, thereby indicating that the thickness of the steel rebars passive film should be within a few nanometers thick [12,32]. The presence of Fe^{2+} can be assigned to magnetite or Fe^{2+} oxides. The ratio of Fe^{2+}/total Fe-oxides are 0.32, 0.34, 0.41, 0.45 for HRB400, 1.5 Cr, 3 Cr and 5 Cr steel, respectively. Literature has shown that the film of carbon steel in alkaline media corresponds basically to a double-layer model consisting of an inner magnetite and outer iron oxides according to Fe_3O_4/Fe^{3+} structure [2,28,32,33]. The most internal layer is composed of Fe^{2+} oxides, which are considered to be more corrosion resistant and able to protect steel rebar from corrosion. From the XPS quantitative analysis, it can be deduced that the addition of Cr elements in the steel may suppress the oxidation of Fe^{2+} to Fe^{3+} in passive films, thus improving the corrosion resistance of the steel rebars.

The chromium profile peaks CrO_3 (578.2 eV) and $Cr(OH)_3$ (577.1 eV) could only be detected in 3 Cr- and 5 Cr- modified steel passive films (Fig. 9), which may be due to the less content chromium in 1.5 Cr steel passive film. Cr elements are involved in the formation of 3 Cr- and 5 Cr-modified steel passive films, and the content of $Cr(OH)_3$ of 5 Cr steel is higher than that of the 3 Cr steel. Cr^{3+} is a key factor for self-repair and the stability of the stainless steel passive film [33,34]. As a result, the passive film stability of 5 Cr-steel is much higher.

Fig. 10 shows the spectra of the passive film formed on HRB400 steel and Cr modified steel in the O1s region. Oxygen species, O^{2-} and OH^-, in passive film play a role of connecting metal ions. O1s spectra are split into three components O^{2-}(530.2 eV), OH^-(531.8 eV) and H_2O (533 eV). It can be seen that OH^- is the primary constituent of the passive film, which corresponds to the formation of FeOOH and $Cr(OH)_3$. While O^{2-} is also the major constituent of the passive film, which corresponds to the formation of FeO.

3.6. AES results

AES analysis was carried out after the immersion in CH solution for 7 days. Fig. 11 shows the AES depth profiling of the oxide

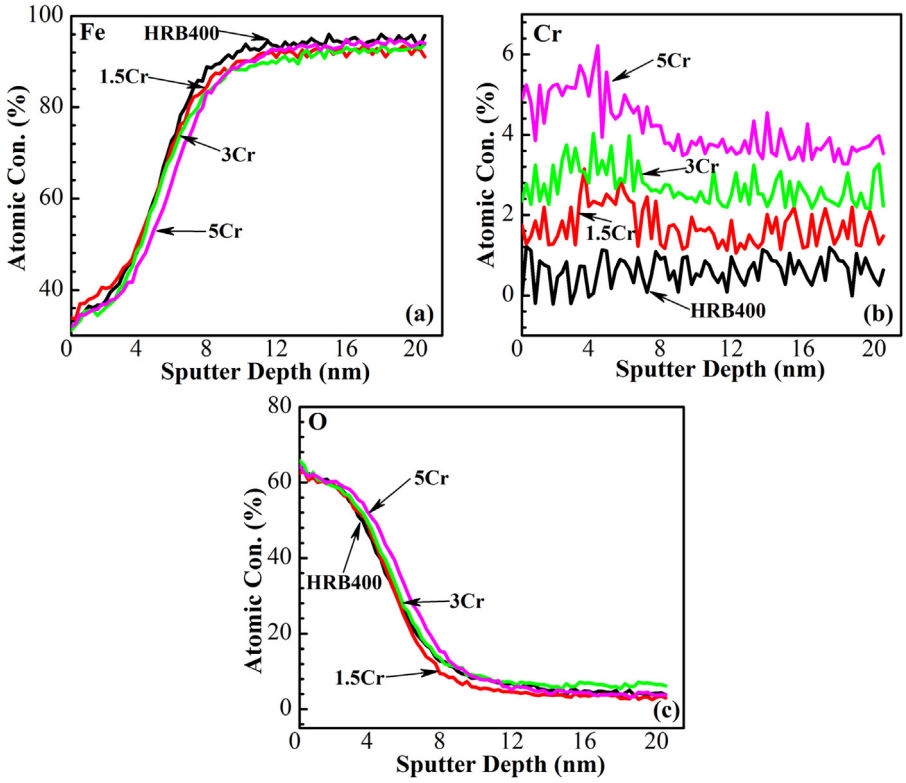

Fig. 11. AES depth profiles of the passive films formed on steel rebars in CH solution: (a) Fe, (b) Cr, (c) O.

films formed after immersion at OCP in CH solution for 7 days. Fig. 11(a) shows that the concentration of Fe in the passive films is approximately 30 at.% at the surface and increases incrementally with the depth. The content of Fe in the passive film declines with the increase in Cr content, which shows that Cr is involved in the formation of a passive film. From Fig. 11(b), because of the slow migration of Cr elements, Cr enrichment is observed at approximately 5 nm in the inside layer of film, which confirms the results of the OCP measurement and EIS analysis. Fig. 11(c) shows that the O concentration rapidly decreases with the extension of the etching time, and the variation does not show any abrupt change. Some researchers [26,35] suggested that the interface of the passive film and the matrix is the position where the O content is half of its maximal value. Thus, the thickness of the steel rebars passive film formed in CH solution is approximately 5–6 nm and increases slightly with the Cr content. 5 Cr steel has the thickest film (5.5 nm). As a result, a relatively thick stable passive film is able to form on the surface of the Cr-modified steel in CH solution.

4. Conclusions

The increasing Cr content decreases the passive film formation rate of steel rebars in CH solution. Stable open-circuit potential could be reached at around −250 mV after immersion for three days in CH solution.

The EIS diagram of steel exhibits a capacitive loop with a one-time constant for 30 min of immersion, and the Cr-modified steel has a larger polarization resistance. When immersed for 6–72 h, the R_f of the Cr-modified low alloy steels is less than that of the HRB400 steel. When immersed for more than 72 h, the R_f tends to stabilize and Cr-modified steels are larger than that of the HRB400 steel. Cr takes part in forming a protective passive film and resulting in a higher R_p. Stable passive film is capable of forming on Cr-modified steel in CH solution.

Fe oxides occupy a dominant position in the passive film. Moreover, Cr oxides exist in 3Cr- and 5Cr-steels. The thickness of the passive film is 5–6 nm and increases slightly with the enhancement of the Cr content. The Fe oxides mainly compose the outer layer of the passive film, and Cr primarily participates in the formation of the inside layer.

Acknowledgments

This work was supported by the National Science and Technology Infrastructure Platforms Construction Project and the National Basic Research Program of China (973 Program project, No.2014CB643300).

References

[1] H.B. Gunay, P. Ghods, O.B. Isgor, G.J.C. Carpenter, X. Wu, Characterization of atomic structure of oxide films on carbon steel in simulated concrete pore solutions using EELS, Appl. Surf. Sci. 274 (2013) 195–202.
[2] P. Ghods, O.B. Isgor, J.R. Brown, F. Bensebaa, D. Kingston, XPS depth profiling study on the passive oxide film of carbon steel in saturated calcium hydroxide solution and the effect of chloride on the film properties, Appl. Surf. Sci. 257 (2011) 4669–4677.
[3] X. Feng, Z. Yu, Y. Tang, X. Zhao, X. Lu, The degradation of passive film on carbon steel in concrete pore solution under compressive and tensile stresses, Electrochim. Acta 58 (2011) 258–263.
[4] N.E. Hakiki, M.F. Montemor, M.G.S. Ferreira, M.D.C. Belo, Semiconducting properties of thermally grown oxide films on AISI 304 stainless steel, Corros. Sci. 42 (2000) 687–702.
[5] H. Luo, C.F. Dong, K. Xiao, X.G. Li, Characterization of passive film on 2205 duplex stainless steel in sodium thiosulphate solution, Appl. Surf. Sci. 258 (2011) 631–639.
[6] L. Freire, M.J. Carmezim, M.G.S. Ferreira, M.F. Montemor, The passive behaviour of AISI 316 in alkaline media and the effect of pH: a combined electrochemical and analytical study, Electrochim. Acta 55 (2010) 6174–6181.
[7] M. Mancio, G. Kusinski, P.J.M. Monteiro, T.M. Devine, Electrochemical and in-situ sers study of passive film characteristics and corrosion performance of 9% Cr microcomposite steel in highly alkaline environments, J. ASTM Int. 6 (2009) 173–188.

[8] H. Luo, C.F. Dong, X.G. Li, K. Xiao, The electrochemical behaviour of 2205 duplex stainless steel in alkaline solutions with different pH in the presence of chloride, Electrochim. Acta 64 (2012) 211–220.
[9] R. Liu, L. Jiang, J. Xu, C. Xiong, Z. Song, Influence of carbonation on chloride-induced reinforcement corrosion in simulated concrete pore solutions, Constr. Build. Mater. 56 (2014) 16–20.
[10] R.G. Duarte, A.S. Castela, R. Neves, L. Freire, M.F. Montemor, Corrosion behavior of stainless steel rebars embedded in concrete: an electrochemical impedance spectroscopy study, Electrochim. Acta 124 (2014) 218–224.
[11] M. Moreno, W. Morris, M.G. Alvarez, G.S. Duffó, Corrosion of reinforcing steel in simulated concrete pore solutions: effect of carbonation and chloride content, Corros. Sci. 46 (2004) 2681–2699.
[12] X. Cheng, Z. Feng, C. Li, C. Dong, X. Li, Investigation of oxide film formation on 316L stainless steel in high-temperature aqueous environments, Electrochim. Acta 56 (2011) 5860–5865.
[13] C.O.A. Olsson, D. Landolt, Passive films on stainless steels-chemistry, structure and growth, Electrochim. Acta 48 (2003) 1093–1104.
[14] D.D. Macdonald, S.R. Biaggio, H. Song, Steady-state passive films; interfacial kinetic effects and diagnostic criteria, J. Electrochem. Soc. 139 (1992) 170–176.
[15] A. Poursaee, C.M. Hansson, Reinforcing steel passivation in mortar and pore solution, Cem. Concr. Res. 37 (2007) 1127–1133.
[16] L. Li, A. Sagüés, Chloride corrosion threshold of reinforcing steel in alkaline solutions-open-circuit immersion tests, Corrosion 57 (2001) 19–28.
[17] M. Liu, X. Cheng, X. Li, Z. Jin, H. Liu, Corrosion behavior of Cr modified HRB400 steel rebar in simulated concrete pore solution, Constr. Build. Mater. 93 (2015) 884–890.
[18] E. Volpi, A. Olietti, M. Stefanoni, S.P. Trasatti, Electrochemical characterization of mild steel in alkaline solutions simulating concrete environment, J. Electroanal. Chem. 736 (2014) 38–46.
[19] S.M.A.E. Haleem, E.E.A.E. Aal, S.A.E. Wanees, A. Diab, Environmental factors affecting the corrosion behaviour of reinforcing steel: i. the early stage of passive film formation in $Ca(OH)_2$ solutions, Corros. Sci. 52 (2010) 1675–1683.
[20] J.M. Abd El Kader, A.M. Shams El Din, Film thickening on nickel in aqueous solution in relation to anion type and concentration, Br. Corros. J. 4 (1979) 40–45.
[21] U.R. Evans, The Corrosion and Oxidation of Metals, London-Edward Arnold, 1960, pp. 248–298.
[22] M. Sánchez, J. Gregori, C. Alonso, J.J. García-Jareño, H. Takenouti, F. Vicente, Electrochemical impedance spectroscopy for studying passive layers on steel rebars immersed in alkaline solutions simulating concrete pores, Electrochim. Acta 52 (2007) 7634–7641.
[23] Y. Wang, Y. Zuo, X. Zhao, S. Zha, The adsorption and inhibition effect of calcium lignosulfonate on Q235 carbon steel in simulated concrete pore solution, Appl. Surf. Sci. 379 (2016) 98–110.
[24] R. Kirchheim, B. Heine, H. Fischmeister, S. Hofmann, H. Knote, U. Stolz, Cheminform abstract: passivity of iron-chromium alloys, Cheminform 20 (1989).
[25] N. Sato, K. Kudo, T. Noda, Single layer of the passive film on Fe, Corros. Sci. 10 (1970) 785–794.
[26] H. Luo, H. Su, C. Dong, K. Xiao, X. Li, Electrochemical and passivation behavior investigation of ferritic stainless steel in alkaline environment, Constr. Build. Mater. 96 (2015) 502–507.
[27] R. Wang, S. Luo, M. Liu, Y. Xue, Electrochemical corrosion performance of Cr and Al alloy steels using a J55 carbon steel as base alloy, Corros. Sci. 85 (2014) 270–279.
[28] N.E. Hakiki, Comparative study of structural and semiconducting properties of passive films and thermally grown oxides on AISI 304 stainless steel, Corros. Sci. 53 (2011) 2688–2699.
[29] J. Williamson, O.B. Isgor, The effect of simulated concrete pore solution composition and chlorides on the electronic properties of passive films on carbon steel rebar, Corros. Sci. 106 (2016) 82–95.
[30] Y. Zhang, Study of the semi-conductive behavior of the passive film on carbon steel in simulated concrete pore solution under stress, Anti-Corros. Methods Mater. 62 (2015) 363–370.
[31] D.A. Shirley, High-resolution X-ray photoemission spectrum of the valence bands of gold, Phys. Rev. B 5 (1972) 4709–4714.
[32] J.M. Deus, L. Freire, M.F. Montemor, X.R. Nóvoa, The corrosion potential of stainless steel rebars in concrete: temperature effect, Corros. Sci. 65 (2012) 556–560.
[33] L. Freire, M.A. Catarino, M.I. Godinho, M.J. Ferreira, M.G.S. Ferreira, A.M.P. Simões, Electrochemical and analytical investigation of passive films formed on stainless steels in alkaline media, Cem. Concr. Compos. 34 (2012) 1075–1081.
[34] Y. Wang, X. Cheng, X. Li, Electrochemical behavior and compositions of passive films formed on the constituent phases of duplex stainless steel without coupling, Electrochem. Commun. 57 (2015) 56–60.
[35] M.G. Faichuk, S. Ramamurthy, W.M. Lau, Electrochemical behaviour of Alloy 600 tubing in thiosulphate solution, Corros. Sci. 53 (2011) 1383–1393.